The role of limestone during fluidized bed oxy-combustion of coal and biomass

Carlos Lupiáñez[a], M. Carmen Mayoral[b], Luis I. Díez [a,1],

Eloy Pueyo[a], Sergio Espatolero[a], J. Manuel Andrés[b]

[a] CIRCE, University of Zaragoza, Campus Río Ebro, 50018-Zaragoza, Spain

[b] Instituto de Carboquímica-CSIC, Miguel Luesma 4, 50018-Zaragoza, Spain

Abstract

The interest in bio-CCS technologies is growing due to their potential to reduce CO_2 emission in power generation. Oxy-co-firing in fluidized-bed units is one of the available techniques to develop bio-CCS, offering wide fuel flexibility and low SO_2 and NO_x emissions. This paper discusses the results of an experimental campaign carried out in a lab-scale fluidized bed reactor. The work focuses on the influence of limestone when oxy-firing blends of lignite and corn stover. Two different types of limestone with two Ca:S molar ratios were tested, and operational conditions were selected to compare the mechanisms governing desulphurization. Emissions of SO_2, NO and HCl, together with deposition rates and ash mineralogy are studied in the paper. SO_2 capture increases with the Ca:S ratio and bed temperature, but to a different extent depending on the limestone fragmentation. The amount of NO emitted rises with the Ca:S ratio and the presence of calcined limestone (indirect desulphurization). The HCl concentration in the gas phase is dominated by alkali sulfation. Finally, the conditions for the highest desulphurization efficiency diminished the deposition rates, but increased the risk for chlorine-induced corrosion.

Keywords

Oxy-combustion, Limestone, Emissions, Deposition, Biomass, Fluidized beds

[1] Corresponding author, e-mail address: luisig@unizar.es

1. Introduction

Among the carbon capture and storage technologies (CCS), oxy-firing is one of the nearly commercially available solutions [1–3]. The investment during the last few years has allowed demonstration-scale facilities to be commissioned in which the feasibility of oxy-firing has been proved [4–7]. Nevertheless, important research efforts are still ongoing concerning its efficiency, emissions and fuel-related issues [8–12].

Oxy-combustion was initially developed and scaled-up in pulverized fuel units, but now oxy-fired fluidized bed boilers are of similar size. The latter offers the additional capability of burning low-rank fuels with good efficiency. This includes combustion of residual biomass, which implies CO_2–neutral power generation [13–15]. Bio-CCS technologies based on the combination of residual biomass combustion and permanent CO_2 removal are considered to be negative emission concepts [16–18].

Despite the use of residual biomass for power generation can result in environmental benefits related to SO_2 and NO_x emissions [19, 20], several operational issues arise related to its mineral matter composition. The release of alkali metals, which are mainly present in herbaceous biomasses, promotes condensation on water-tube surfaces, limiting the heat transfer efficiency. Additionally, alkali chlorides in deposits interact with Fe and Cr, accelerating corrosion of heat exchangers in boilers [21–24]. In the case of fluidized bed units, interactions with silicates (in the sand) increase the risk of bed agglomeration. To reduce these difficulties, some researchers have explored the addition of alumina, dolomite, kaolin or limestone in the bed inventory [14].

The co-combustion of coal and residual biomass has been found to decrease agglomeration and corrosion risks compared to firing biomass alone [25–27]. The effectiveness of co-firing in preventing deposition of alkali chlorides is due to sulphur in coal since SO_2 and SO_3 react with alkali chlorides, yielding alkali sulphates (R.1, R.2):

$$2\,MCl + SO_2 + H_2O + {}^1\!/_2\,O_2 \rightarrow M_2SO_4 + 2\,HCl \quad \text{(R. 1)}$$

$$2\,MCl + SO_3 + H_2O \rightarrow M_2SO_4 + 2\,HCl \quad \text{(R. 2)}$$

These mechanisms reduce the interaction between the bed material and alkali metals, lessening the deposition of alkali chlorides [28]. The formation of alkali sulphates is not

desirable from the point of view of heat transfer since fouling may be increased, but at least the risk of tube corrosion is reduced.

In fluidized bed reactors, SO_2 and SO_3 available for (R. 1) and (R. 2) are usually limited by in-situ desulphurization due to sorbent addition, generally limestone. Depending on the operational conditions, desulphurization can be carried out following two different mechanisms. When limestone is calcined, yielding CaO (R. 3), it retains SO_2 following reaction (R. 4):

$$CaCO_3 \leftrightarrow CaO + CO_2 \quad \text{(R. 3)}$$

$$CaO + SO_2 + {}^1/_2\, SO_2 \rightarrow CaSO_4 \quad \text{(R. 4)}$$

This two-step mechanism, also called indirect capture, is typically found in atmospheric fluidized beds under conventional combustion. However, under oxy-firing conditions, with higher CO_2 concentrations, calcination can be inhibited [29] and SO_2 reacts with $CaCO_3$ by means of a direct capture mechanism (R. 5):

$$CaCO_3 + SO_2 + {}^1/_2\, O_2 \rightarrow CaSO_4 + CO_2 \quad \text{(R. 5)}$$

At typical bed temperatures (~850 ºC), direct capture is the governing mechanism for SO_2 retention. Direct capture is slower than indirect desulphurization mainly due to the smaller pores of limestone compared to those of lime, so this process is controlled by the diffusion of SO_2 in the particle and in the product layer [30]. Accordingly, other studies have found that indirect capture offers the highest desulphurization efficiencies also under oxy-firing conditions, but for an optimum temperature in the range of 900-925ºC [31, 32].

On the other hand, some researchers have investigated the effect of co-firing in O_2/CO_2 atmospheres. Skeen et al. [33] studied the effect of co-firing sawdust and coal in a pulverized burner, reporting a sharp increase in emissions of NO with the O_2 concentration in the primary oxidizer stream. Riaza et al. [34] added biomass to coal in an entrained-flow reactor to study ignition and NO emission. Moroń and Rybak [35] and Pickard et al. [36] reported a reduction of NO_x and SO_2 emissions during co-firing under O_2/CO_2 atmospheres. Jurado et al. [37] highlighted the relevance of increasing the concentration of corrosive substances due to recycled flue gases, while Ekvall et al. [38,

39] injected KCl into a pulverized fuel reactor, obtaining a higher alkali sulfation in oxy-firing mode than in air-firing mode.

Nevertheless, there are few experiences to date concerning oxy-firing of coal and biomass in fluidized bed facilities. Tan et al. [40] conducted oxy-co-firing experiments to demonstrate the viability of this technology and characterize pollutant emission. Duan et al. [41] focused on NO_x emission, observing dependencies similar to oxy-firing of coal alone. Kosowska-Golachowska et al. [42] studied the influence of the fluidizing gas composition in combustion, reducing burn-out time and increasing temperature with the highest O_2 concentration.

There is a lack of research addressing oxy-firing of coal with residual biomass in fluidized bed reactors, and this paper aims to increase knowledge in this field. In particular, there are no reported works regarding the influences of limestone and the desulphurization mechanisms when coal and biomass are fired together. This paper describes and discusses the experimental results of oxy-firing campaign with lignite and corn stover, encompassing gaseous emissions, the ash composition and the characterization of deposits.

2. Experimental setup

2.1. Experimental facility

The experimental campaign was conducted in a 100 kW_{th} fluidized bed. Figure 1 shows an updated scheme of the plant after a recent refurbishment. The height of the reactor is 3 500 mm, and the inner diameter is 205 mm. The unit can be operated under air-firing and oxy-firing modes, using O_2/CO_2 mixtures from commercial gas cylinders. The bed temperature is controlled by means of four water-cooled probes, whereas the freeboard is electrically heated to maintain the temperature. Fuels and sorbents are fed from hoppers by means of independent screw feeders.

The operational parameters are measured by thermocouples, pressure sensors and flow-meters and are continuously recorded. The flue-gas composition is provided on-line by a gas analyser. CO, CO_2, SO_2 and NO concentrations are measured by NDIR (non-dispersive infrared) sensors. A paramagnetic sensor is used to measure O_2

concentration. The measurement uncertainties are 1% for the temperature sensors, 2% for the pressure sensors and 1% for the gas analyser cells.

To simulate deposition on the superheater tubes, an air-cooled probe can be inserted at 800, 2 000 or 3 300 mm over the distributor plate. A removable coupon made of AISI Type 304 stainless steel is placed in the tip of the probe for further SEM-EDX analysis of the deposits. The probe is equipped with a thermocouple and a PID controller, which determines the air flow-rate required to maintain the prescribed surface temperature.

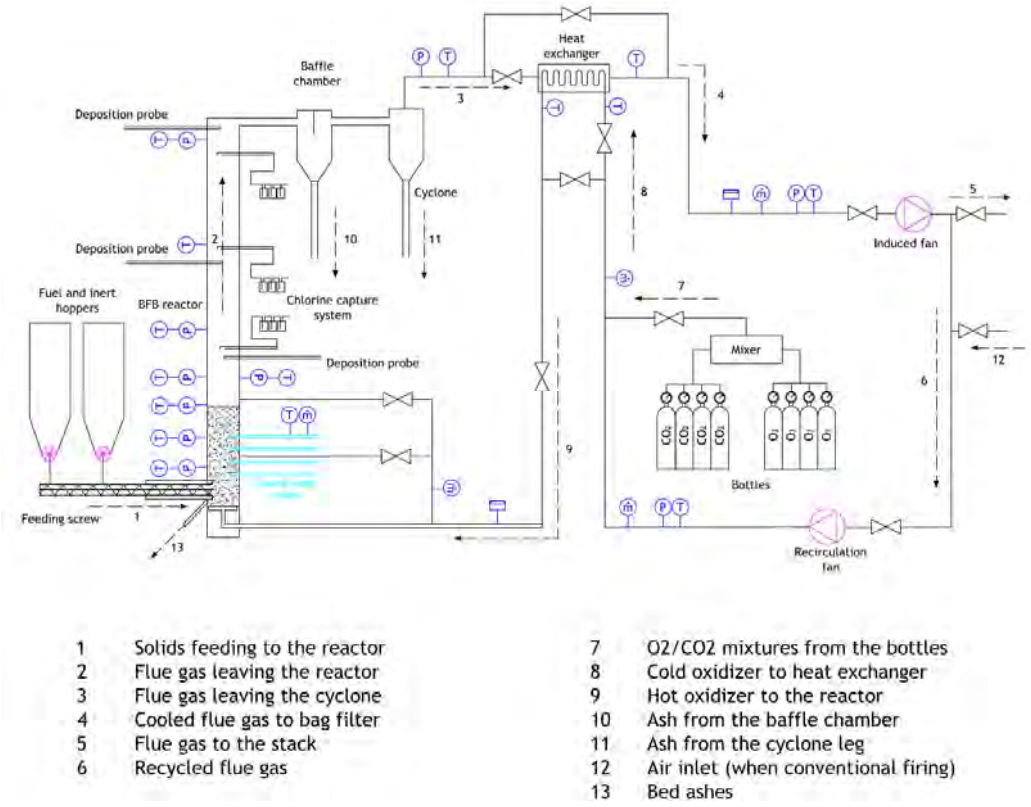

Figure 1. Oxy-fired fluidized bed facility.

Gas samples can be taken while on-load at 800, 2 000 and 3 100 mm over the distributor plate. Each sample is conveyed through three impingers with a 0.1 M Na_2CO_3 solution that retains chlorides, fluorides, sulphates and nitrates. The chlorine concentration in the impinger solution is determined by ion chromatography. Solids can also be gathered while on-load from the bed bottom, the baffle chamber and the cyclone.

133 *2.2 Fuels and sorbents*

134 The coal selected for the experiments was Spanish lignite, which has a very high
135 sulphur and ash content (see Table 1). The mean particle size was 0.7 mm, with particle
136 sizes between 0.3 and 1.0 mm.

	Lignite	Corn Stover
Proximate analysis (%wt.)		
Moisture	13.57	6.18
Ash	30.30	5.50
Volatiles	25.72	70.68
Fixed carbon	30.41	17.64
Ultimate analysis (%wt.)		
C	40.53	43.30
H	3.18	5.82
N	0.28	0.57
S	6.65	0.11
Cl	–	0.35
LHV (kJ/kg)	14 434	15 438
Ash (%wt.), by ICP		
Al_2O_3	26.01	1.36
CaO	3.27	8.72
Fe_2O_3	22.23	6.08
K_2O	0.92	27.90
MgO	0.96	3.27
Na_2O	0.12	0.22
SiO_2	41.06	29.81
TiO_2	0.76	0.80
P_2O_5	–	3.81
MnO_2	–	0.14

137 **Table 1.** Fuel analysis, heating value and ash composition, as received.

138

139 Corn stover, with 0.35% chlorine content as received, was the herbaceous biomass
140 selected for the experiments. Aiming to test the influence of the chlorine content, the
141 corn stover was doped with a KCl solution to increase the concentration up to 1% Cl.
142 The apportioned KCl was dispersed onto the biomass surface as 1 μm crystals identified
143 by SEM (Figure 2). For that particle size, it has been claimed that in-flight sulfation is

achievable at the short gas residence times typical of combustion systems [43]. The resulting biomass was ground and sieved to obtain a fraction between 1.0 and 2.0 mm.

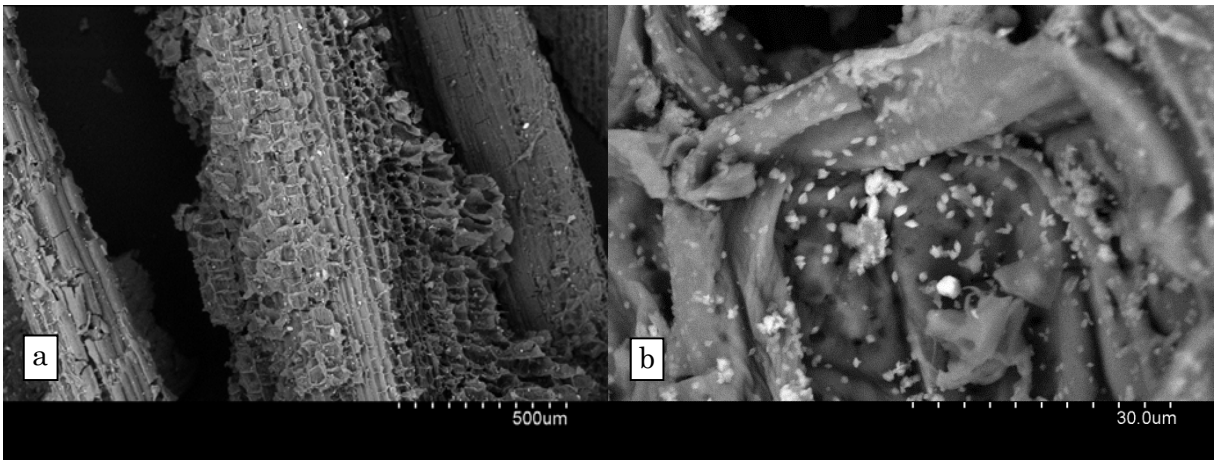

Figure 2. (a) SEM micrograph of KCl doped biomass, (b) detailed micrographs of surface KCl crystals.

As regards the sorbents, two domestic limestones with high $CaCO_3$ contents (> 97%) were selected: Granicarb limestone and Bahoto limestone. The mean particle size was approximately 0.6 mm for both. Silica sand was the inert constituent of the bed at the beginning of each test, with the same mean particle size.

2.3 Experimental conditions

A total set of six tests were conducted burning a blend of lignite and corn stover, with a coal/biomass ratio of 70/30% on an energy basis. Table 2 summarizes the experimental conditions during the tests.

The first test was run under air-firing conditions at a bed temperature of 850 ºC. The other five tests were run under oxy-firing conditions with a 35/65% O_2/CO_2 mixture. To study the influence of the desulphurization mechanism during the oxy-firing tests, the bed temperature was modified from 850 ºC (direct capture, non-calcining conditions) to 925 ºC (indirect capture, calcining conditions). A reference molar ratio of Ca:S = 6 was adopted due to the high sulphur content of the coal and the execution of tests under non-calcining conditions (lower desulphurization efficiencies could be expected). The molar ratio was decreased to 2 for a single test to discuss its effect under calcining conditions. Four tests were conducted with Granicarb limestone, the rest with Bahoto limestone.

In the present paper, the experiments are named according to the experimental conditions: first, the combustion mode is noted as air-firing (A) or oxy-firing (O); second, the limestone type is indicated as Granicarb (G) or Bahoto (B); third, the Ca:S molar ratio is either 2 or 6; and finally, the desulphurization mechanism is either indirect (I) or direct (D). During all of the experiments, the deposition probe and chlorine capture system were inserted into the highest ports at the top of the freeboard. The deposition probe temperature was set at 450 ºC.

Test #	Fluidizing gas	Limestone	Ca:S	Bed temperature	Desulphurization mechanism
A-G6I	Air	Granicarb	6	850 ºC	Calcining
O-G6D	35/65% O_2/CO_2	Granicarb	6	850 ºC	Non-calcining
O-G6I	35/65% O_2/CO_2	Granicarb	6	925 ºC	Calcining
O-G2I	35/65% O_2/CO_2	Granicarb	2	925 ºC	Calcining
O-B6D	35/65% O_2/CO_2	Bahoto	6	850 ºC	Non-calcining
O-B6I	35/65% O_2/CO_2	Bahoto	6	925 ºC	Calcining

Table 2. Experimental conditions during the tests.

2.4 Experimental techniques

Solid samples were studied by means of scanning electron microscopy in a Hitachi S-3400N device, in which micrographs of selected surfaces were taken by a retro-dispersive electron detector for morphology characterization. The chemical composition of selected surfaces and mapping were performed by means of EDX in a Rontec XFlash detector. X-ray diffraction (XRD) was used to determine the phase composition of the crystalline species in a Siemens Bruker D8 Advance diffractometer set for CuKα radiation. The diffraction angle scanned was 20–60° (2 θ) using a step size of 0.05° (2 θ).

3. Results and discussion

3.1. Emissions

Table 3 shows the mean values and standard deviations for the freeboard temperature and flue gas concentrations recorded on-line during the tests (the concentrations were

normalized to 6% O_2). The table also includes the calculated desulphurization efficiency and HCl concentration in the freeboard.

	A-G6I	O-G6D	O-G6I	O-G2I	O-B6D	O-B6I
T_{fb} (ºC)	793 ± 10	791 ± 9	700 ± 17	721 ± 8	794 ± 10	798 ± 8
O_2 (%)	7.53 ± 0.55	7.72 ± 0.38	7.93 ± 0.75	7.87 ± 1.30	7.62 ± 0.81	12.72 ± 1.97
CO (mg/Nm³)	386 ± 28	209 ± 10	189 ± 16	186 ± 29	380 ± 40	43 ± 10
NO (mg/Nm³)	149 ± 19	399 ± 58	530 ± 69	412 ± 58	348 ± 57	510 ± 42
SO_2 (mg/Nm³)	331 ± 32	13950 ± 745	3151 ± 345	8187 ± 910	2181 ± 351	824 ± 72
NO (mg/MJ)	27.7	39.9	54.1	39.6	35.9	49.1
SO_2 (mg/MJ)	66	1488	354	843	246	86
Eff. Desulph (%)	97.9	54.1	89.1	74.0	92.4	97.4
HCl (mg/Nm³)	67	243	155	211	116	85

Table 3. Freeboard temperature; CO, NO and SO_2 emissions (normalized to 6% O_2); desulphurization efficiency; and HCl concentration.

3.1.1. SO_2 emissions

The experimental campaign with Granicarb limestone confirms the expected results. The desulphurization efficiency obtained from the test under conventional combustion (A-G6I) reached a value of almost 98%; this is explained by the calcining conditions and bed temperature being within the optimum range for SO_2 capture [44].

The change to the direct desulphurization mechanism in test O-G6D, as a consequence of the high CO_2 concentration, yielded an important increase of emitted SO_2 and a consequent drop of the desulphurization efficiency to 54%. This observation is consistent with the results found by de Diego et al. [31, 45] and Wu et al. [46]. These researchers reported lower efficiencies as a consequence of the lower porosity of the non-calcined sorbent (for typical particle sizes in fluidized beds).

Oxy-fired tests O-G2I and O-G6I were carried out again under calcining conditions since the bed temperature was increased to 925ºC (see also Table 2), leading to an important increase in the desulphurization efficiency in comparison to the O-G6D tests, even in the case of decreasing the molar ratio of Ca:S to 2. A similar behaviour was found by Jia et al. [47] during the operation of an oxy-fired CFB plant at high temperature.

If test A-G6I is compared to O-G6I, the desulphurization efficiency is almost 8 points lower in the case of oxy-firing. An explanation for this reduction was given by Valverde and co-workers [48]. They determined that the pores formed under oxy-firing conditions during calcination were smaller due both to the higher temperatures and CO_2 concentrations.

The use of Bahoto limestone in the last two tests resulted in an increase of the desulphurization efficiency to over 90%. Again, the efficiency is better when operating under calcining conditions. If test O-G6D is compared to test O-B6D, the increase in efficiency is quite outstanding, i.e., from 54.1% to 92.4%. This behaviour is mainly related to the severe fragmentation suffered by the Bahoto limestone, according to the samples taken in the circuit hoppers. The amount of solids collected after the Bahoto test was five times higher than that after the Granicarb test, pointing out a significant increase in the elutriation rates (despite the fluidization velocity remaining the same). These fragmentation conditions were also confirmed by particle micrographs, as shown in the following section. Since the molar ratio Ca:S is sufficiently high, higher limestone fragmentation means a larger surface available to capture SO_2.

3.1.2. NO emissions

The lowest NO emission was detected for the air-fired test, A-G6I. If compared to the corresponding test using oxy-firing, O-G6I, emissions are doubled (in normalized units, mg/MJ, to avoid the effect of the atmosphere). This is not only an effect of the O_2 concentration but also of the lower CO level for the O-G6I test.

The increase in emissions from O-G6D (399 mg/Nm^3) to O-G6I (530 mg/Nm^3) is explained by the presence of calcined limestone rather than the temperature. Despite the increase in temperature that promotes calcining conditions, the effect is attenuated since the freeboard temperature was kept at a lower value (see Table 3). For similar mean temperatures, the difference in emissions was then mainly caused by calcined limestone, with almost the same O_2 and CO concentrations for both tests. This effect has also been observed for conventional coal combustion (i.e., calcining conditions). De Diego et al. [49] reported that NO emission doubled after the addition of limestone in a fluidized bed. Ziljma et al. [50–52] found an important increase of NO due to calcined limestone; the increase progressively slowed down as $CaSO_4$ was formed. Liu and Gibbs

[53] studied how limestone affected the emitted NO in the case of char combustion. On the other hand, Hansen et al. [54] and Lupiáñez et al. [55] showed the limited catalytic effect of fresh limestone in comparison to calcined limestone.

The same result is obtained when Bahoto limestone is supplied (test O-B6D vs. O-B6I), but to an even larger extent. This is also due to the higher O_2 excess and lower CO concentration during the last test.

3.1.3. HCl in gas phase

The HCl concentration in the gas phase was estimated from the gas samples taken at the top of the freeboard and retained in the impingers. HCl is an indicator of alkali sulfation, see reactions (R. 1) and (R. 2). This can be relevant when firing high-sulphur coal together with high-chlorine biomass. According to the results shown in Table 3, the trend is clear: the higher the SO_2 concentration in the flue gases, the higher the HCl concentration detected (due to the enhancement of the sulfation of alkali chlorides). This trend is shown in Figure 3, which clearly shows the relationship. In consequence, in-bed desulphurization determines the release of HCl. The larger amount of chlorine in the gas phase is expected to reduce the presence of chlorine in the deposits as condensed alkali chlorides.

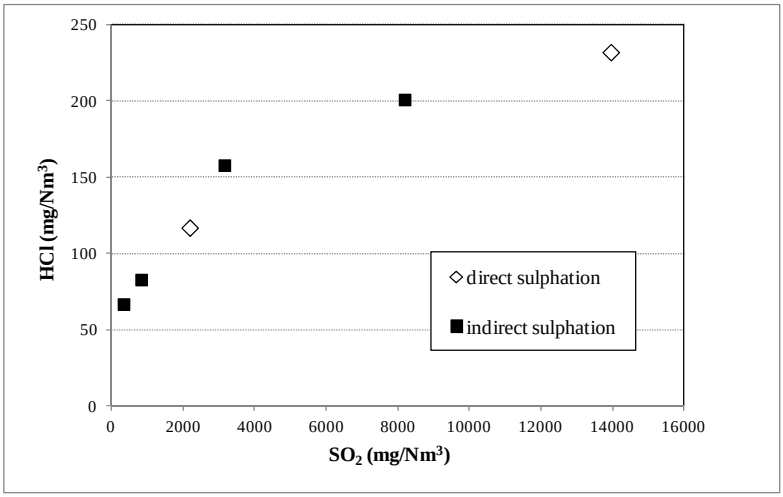

Figure 3. Correlation between HCl and SO_2 in the gas-phase.

Aside from sulfation, HCl can also be released by alkali silication or aluminosilication [25, 56], according to reactions (R. 6) and (R. 7):

$$2\,MCl + nSiO_2 + H_2O \rightarrow M_2O \cdot n\,SiO_2 + 2\,HCl \quad \text{(R. 6)}$$

$$2\,MCl + (nSiO_2 + Al_2O_3) + H_2O \rightarrow 2\,MAlSi_{n/2}O_{(n+2)} + 2\,HCl \quad \text{(R. 7)}$$

The extent of this mechanism is discussed in the following section when the characterization of ash and deposits is addressed.

In brief and regarding emissions in general, the type of limestone used has been revealed to have a large effect on the control of pollutants (SO_2, NO_x). In comparison to air, shifting to an O_2/CO_2 atmosphere was found to increase emissions. Regarding the control of SO_2, the O_2/CO_2 effect can be balanced by increasing the molar ratio of Ca:S or the temperature, but then, NO_x formation can be catalysed if free lime is available. At that point, non-calcining operation can be recommended to jointly control SO_2 and NO_x in oxy-fired units since desulphurization efficiencies over 90% can be achieved, as our work shows.

The selection of the limestone must also take into account its fragmentation propensity, since it is a very influential factor on emissions. Future industrial developments will face a trade-off: the larger the fragmentation rate, the higher the SO_2 capture capability, but the greater the issues related to elutriation, erosion and fouling. The addition of an herbaceous biomass at a limited ratio contributes to reducing pollutants, but its impact on fouling/corrosion must also be assessed.

3.2. Ash composition

3.2.1 Bottom ash

The bottom solids are mainly composed of the initial silica sand, partially sulphated sorbent particles and fuel ash. Visual inspection confirmed that none of the experiments presented agglomerated particles, despite the 30% of corn stover in the blend and high temperature (925º C) during some experiments. The presence of calcite and some refractory elements from lignite ash contributes to the avoidance of agglomeration [27].

The incidence of coating formation was demonstrated by the surface SEM-EDX of the bottom solids. Figure 4 is a micrograph of a representative sand-bed particle, the surface composition of which, also shown in the Figure, indicates the attachment of

298 submicron-sized particles, mainly calcium-based fines and Al and Fe from the coal
299 mineral matter, which does not involve a risk of agglomeration.
300

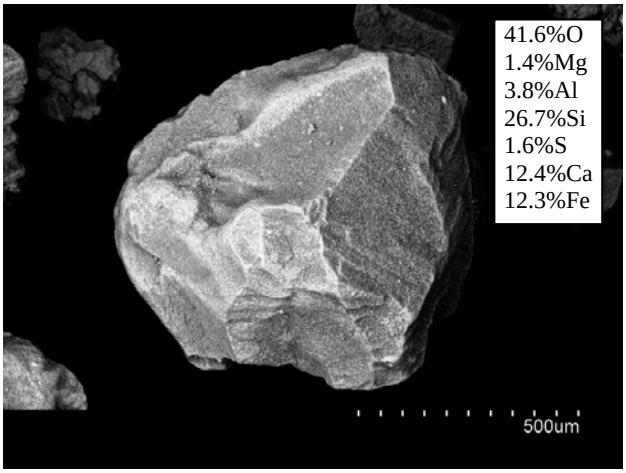

301

302 **Figure 4.** SEM surface micrographs of a sand particle (test O-B6D) and the EDX composition.

303 Table 4 shows the composition determined by SEM-EDX of fuel ash particles (which are
304 identified by the similar silicon-to-aluminium ratio than in the original ash). Tests with
305 direct sulfation present higher percentages of surface Ca than tests in which limestone
306 is initially calcined and are higher in the case of Bahoto limestone due to its greater
307 degree of fragmentation. This fact could be an indication that submicron $CaCO_3$ is more
308 prone to attach to bed particles than CaO. The formation of coating layers hinders the
309 study of other surface reactions, such as potassium silication (R. 6) and
310 aluminosilication (R. 7), compared to the surface K/Al ratios [57]. For this reason, in the
311 present work, the surface K/Al ratios, on an atomic basis, were only calculated for tests
312 under calcining conditions, showing lower surface calcium (see Table 4). The values
313 obtained (0.21–0.27) note the incidence of potassium retention by aluminosilication on
314 ash particles to a similar extent and irrespective of the desulphurization efficiency.
315

	Mg	Al	Si	S	K	Ca	Fe	K/Al
O-G6D	1.95	24.44	30.5	5.62	5.77	16.78	14.94	-
O-G6I	2.62	27.17	29.83	0.00	10.70	8.00	21.59	0.27
O-G2I	2.66	16.90	17.89	1.11	6.29	8.64	46.51	0.25
O-B6D	3.66	14.99	16.60	3.27	1.08	30.00	30.38	-
O-B6I	2.09	23.34	26.01	2.29	7.10	9.83	29.34	0.21

316 **Table 4.** EDX surface elemental composition (%wt.) of bottom solids and the K/Al ratio.

Potassium penetration was studied by EDX and q-mapping of K in cross sections (see Figure 5). The micrograph images of fuel ash after tests A-G6I (Figure 5.a) and O-B6D (Figure 5.b) show the morphology of the ash particles, with cracks, voids and pores related to the original coal texture and its evolution with combustion. Bright iron clusters from inherent pyrite and well-defined quartz crystals are also seen along the cross section. The potassium q-maps are overlapped onto selected areas. They indicate the presence of potassium in the external core of particles, which confirms the reaction of KCl with reactive Si and Al oxides on the ash surfaces, following (R. 6) and (R. 7). The penetration of K is studied by the EDX composition of a number of spots along the particles.

Figure 5.c shows the relative percentage of potassium K / (Al+Si+K+Ca+Fe) related to the depth of penetration. Potassium can be found in the external 50 μm of the ash particles in both tests performed at 850ºC, with a clear relationship with the ash texture, and to a similar extent for the different combustion conditions (air vs. oxy-firing or indirect sulfation vs. direct).

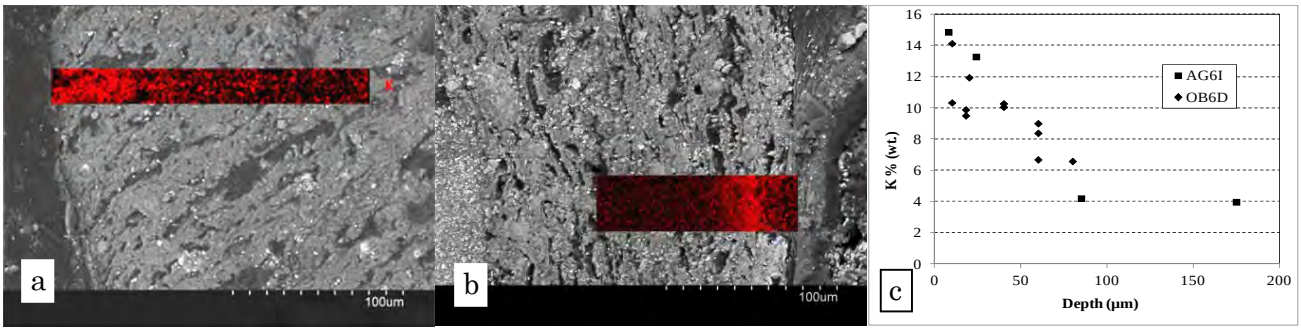

Figure 5. Q-map of samples from tests A-G6I (a) and O-B6D (b), and the relative K content (c).

Sorbent particles were also studied by SEM-EDX. The Granicarb sorbent presents a dense and compact morphology after combustion (Figure 6.a). Line-scanning, elemental mapping and EDX of the sample shown in Figure 6.b were used to demonstrate that sulfation followed an unreacted core model, leading to pore plugging [58]. On the contrary, the Bahoto limestone structure is more porous and presents a high degree of fracture, as presented in Figure 6.c, showing a network sulfation mode [59] for those particles remaining in the bed.

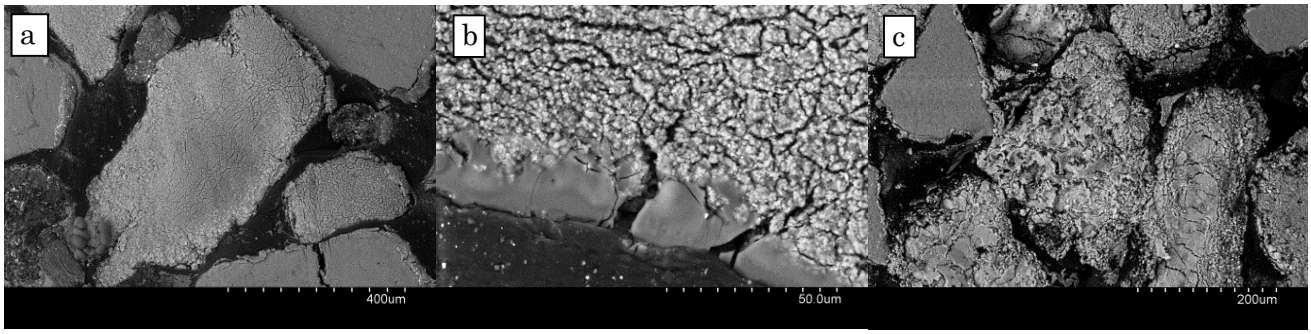

Figure 6. Granicarb sorbent in the bottom bed after test A-6GI (a) and a detailed micrograph of its surface (b); Bahoto sorbent in bottom bed after test O-6BD (c).

Aside from the desulphurization mechanism and its effect on the characterization of sorbent particles, no relevant influence of the type of limestone has been found for bottom ash.

The chemical characterization of sorbent particles also indicated the absence of chlorine. Chlorination of limestone (R.8) or lime (R.9) could be expected due to the presence of HCl in the gas-phase [60]:

$$CaCO_3 + 2\,HCl \leftrightarrow CaCl_2 + H_2O + CO_2 \quad \text{(R. 8)}$$

$$CaO + 2\,HCl \leftrightarrow CaCl_2 + H_2O \quad \text{(R. 9)}$$

Nevertheless, sulfation of lime or limestone (R.4 and R.5) is favoured in simultaneous presence of SO_2 and HCl in the gas-phase at 850ºC [61], reducing the extent of calcium chlorination. This also limits the agglomeration risk caused by the interaction of chlorine with the bed materials.

3.2.2 Fly ash

The samples obtained in the cyclone for each test were studied by EDX. The elemental surface composition (excluding C and O) of the powders is shown in Table 5 for tests with Ca:S = 6. The occurrence of Al, Si and Fe denotes the presence of fuel ash. The amount of calcium in A-G6I and O-B6I samples is high. This could be an indication of sorbent elutriation. Apportioning of the Ca species in the cyclone solids was performed by XRD (Figure 7).

	Mg	Al	Si	S	K	Cl	Ca	Fe
A-G6I	1.35	5.68	8.88	7.10	1.78	1.08	57.53	16.56
O-G6D	2.35	20.00	31.61	6.60	1.13	0.00	15.50	22.80
O-G6I	0.00	12.94	30.55	6.62	2.62	0.00	16.92	30.34
O-B6D	1.54	13.70	23.28	4.85	1.22	0.00	19.89	35.52
O-B6I	1.95	5.72	10.74	10.06	1.89	0.00	56.20	13.44

Table 5. EDX surface elemental composition (%wt.) of cyclone solids.

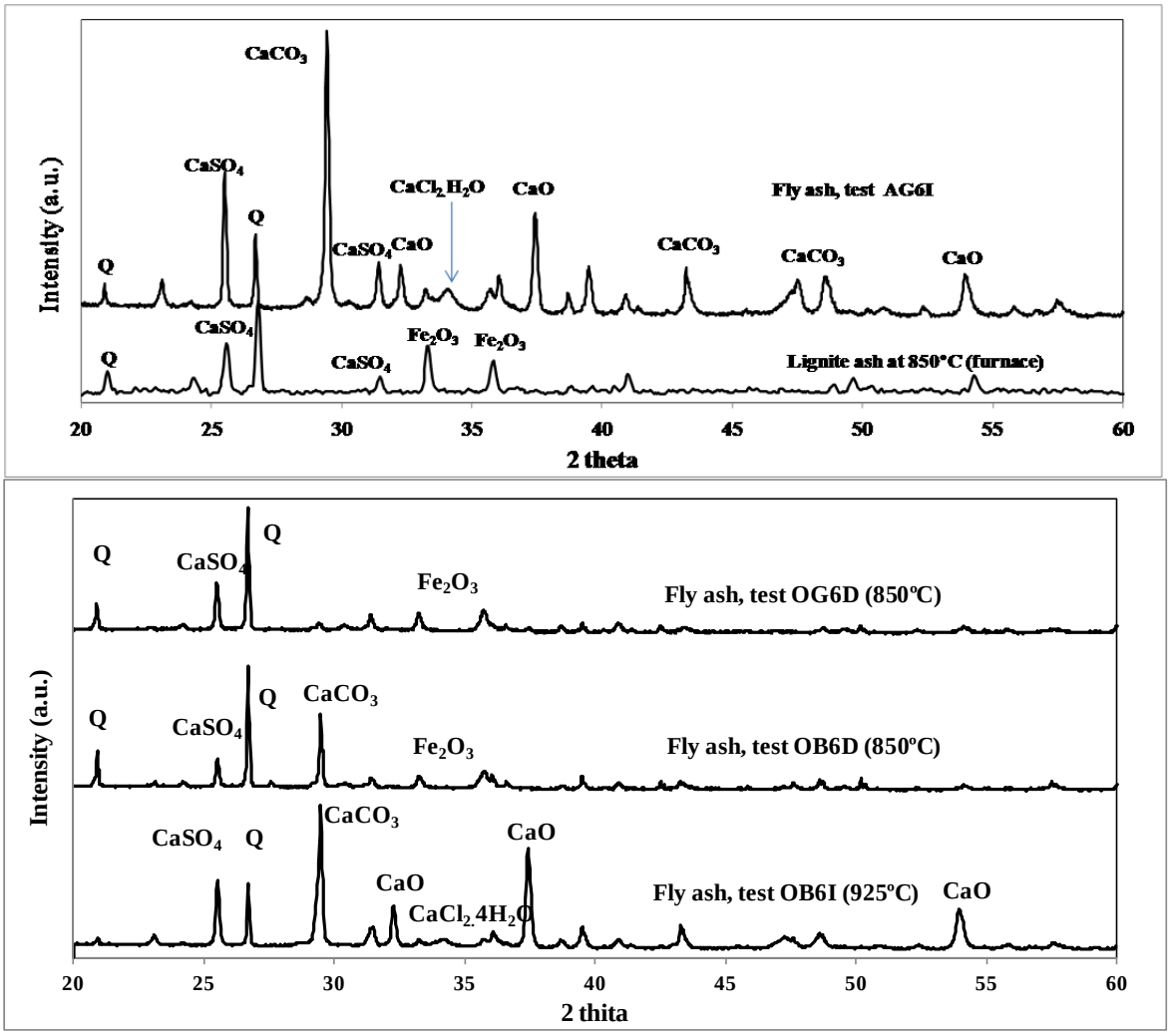

Figure 7. XRD composition of cyclone solids from tests A-G6I, O-G6D, O-B6D and O-B6I.

Sulphated sorbent ($CaSO_4$) and fuel ash (quartz and hematite) are present in all samples. It is worth mentioning that the quartz peak is compatible with evolution with

377 the temperature of the original mineral matter in coal. In Figure 7, it is possible to see
378 that the XRD of lignite coal ash obtained in a muffle furnace (in air, at 850 ºC) gives a
379 major peak for quartz, whereas the initial aluminosilicate is not detected and hematite
380 peaks are observed as oxidation products from the original pyrite.

381 The presence of unreacted limestone is clear in both the Bahoto tests and also for O-
382 B6I, which is evidence that sorbent fragmentation occurs prior to calcination. CaO is
383 present for those cases carried out under indirect sulfation conditions (A-G6I and O-B6I
384 tests), along with a small $CaCl_2 \cdot 4H_2O$ peak, indicating partial chlorination of lime after
385 reaction (R. 8) in SO_2-depleted flue gas. EDX detected the presence of chlorine in A-G6I
386 fly ash, but chlorine is under the detection limit in O-B6I fly ash (see Table 5). This fact
387 is indicating that chlorination of lime is favoured at 600 ºC in air combustion whereas it
388 is limited in oxy-combustion due to competition with recarbonation of the available
389 reactive calcium [62].

390 *3.3. Deposition*

391 Figure 8 shows the deposition coupons obtained after the six experiments. The coupons
392 were analysed by SEM-EDX, as received.

393 The morphology of the deposits could be observed by SEM (Figure 9). The elemental
394 composition of selected 20 μm × 20 μm surface areas was obtained by EDX. Deposits
395 consisted of condensed particles in the micron range, together with particles of ash and
396 bed material. Compositions excluding elements C, O and Fe are given in Table 6.

397 EDX revealed that the main elements present are Ca, K and S, whereas chlorine was
398 only detected in the A-G6I and O-B6I deposits. This is consistent with the lowest HCl
399 concentrations in the gas-phase detected for those tests, which were related to the
400 highest desulphurization efficiencies (over 97%).

401 Apportioning to the different salts cannot be performed according to the elemental
402 composition, so for those cases in which deposits could be removed from the coupon,
403 XRD characterization was performed, as shown in Figure 10. XRD confirmed the
404 presence of both KCl and $CaCl_2$ in the deposition coupon of A-G6I, which was not found
405 for tests O-G6I, O-G2I and O-B6D (as expected according to Table 6). Coupons from the
406 test performed with Bahoto limestone showed an important presence of $CaCO_3$ due to

fragmentation. $CaSO_4$ from sulfation was present in all coupons, as well as potassium sulphate– identified as $K_3H(SO_4)_2$.

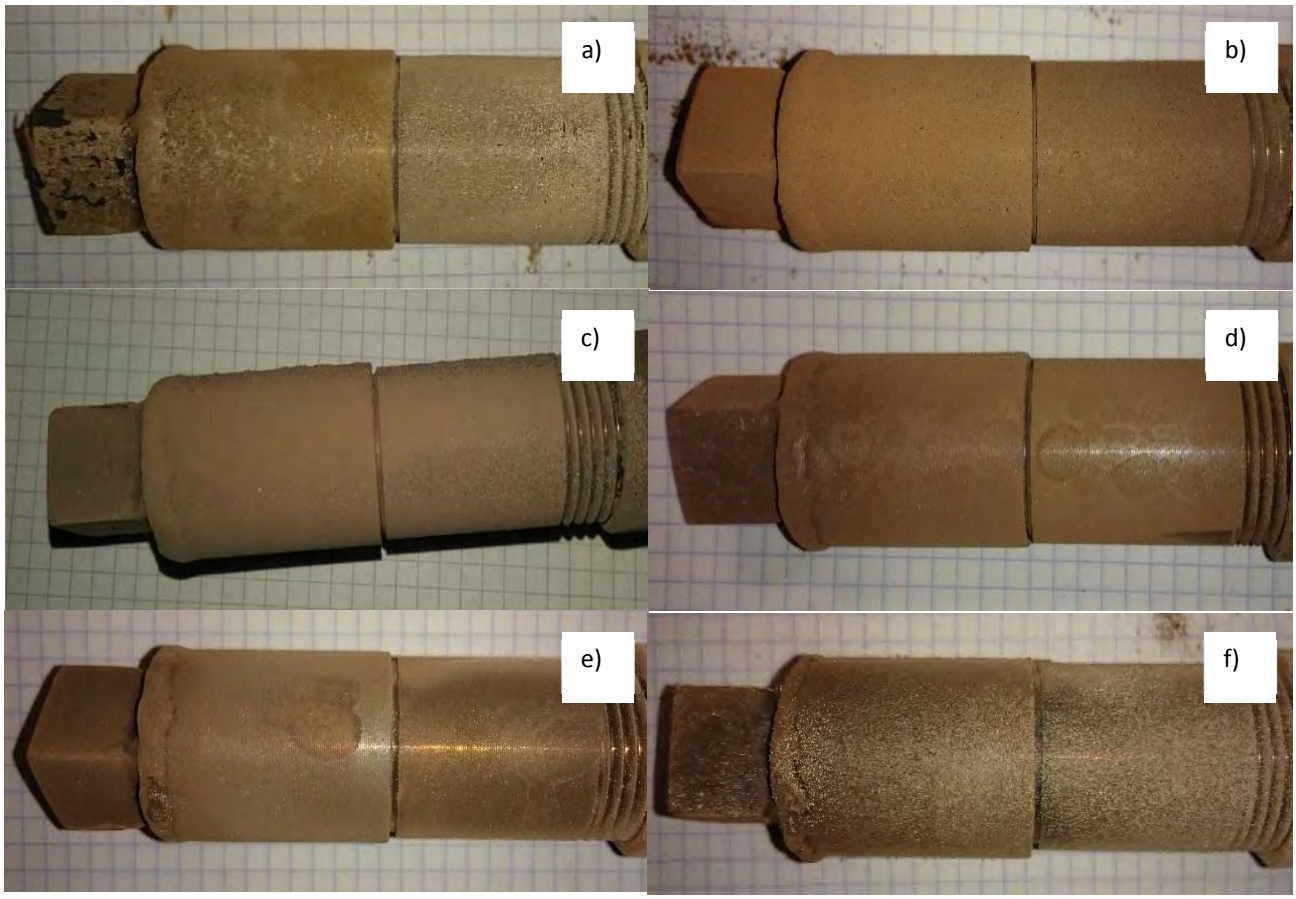

Figure 8. Deposition probes after tests: a) A-G6I, (b) O-G6D, (c) O-G6I, (d) O-G2I, (e) O-B6D, (f) O-B6I.

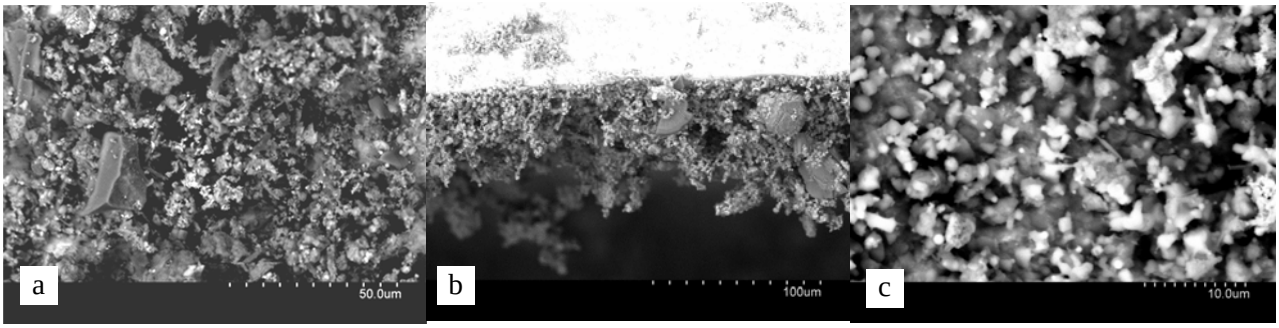

Figure 9. SEM micrographs of deposits from tests: (a) O-G6D, (b) O-G6I, (c) O-6BI.

	Na	Mg	Al	Si	S	K	Cl	Ca
A-G6I	0.00	1.78	5.19	10.89	12.40	8.42	12.97	48.36
O-G6D	0.00	1.58	15.89	20.74	22.42	4.72	0.00	34.64
O-G6I	0.00	0.92	7.12	11.31	22.56	12.69	0.00	41.20
O-G2I	0.00	1.96	9.21	12.42	27.57	29.63	0.00	19.67
O-B6D	0.00	0.00	12.21	16.25	21.19	33.53	0.00	16.82
O-B6I	0.64	1.06	4.13	4.23	18.73	38.35	15.07	17.83

Table 6. EDX surface elemental composition (%wt.) of deposits.

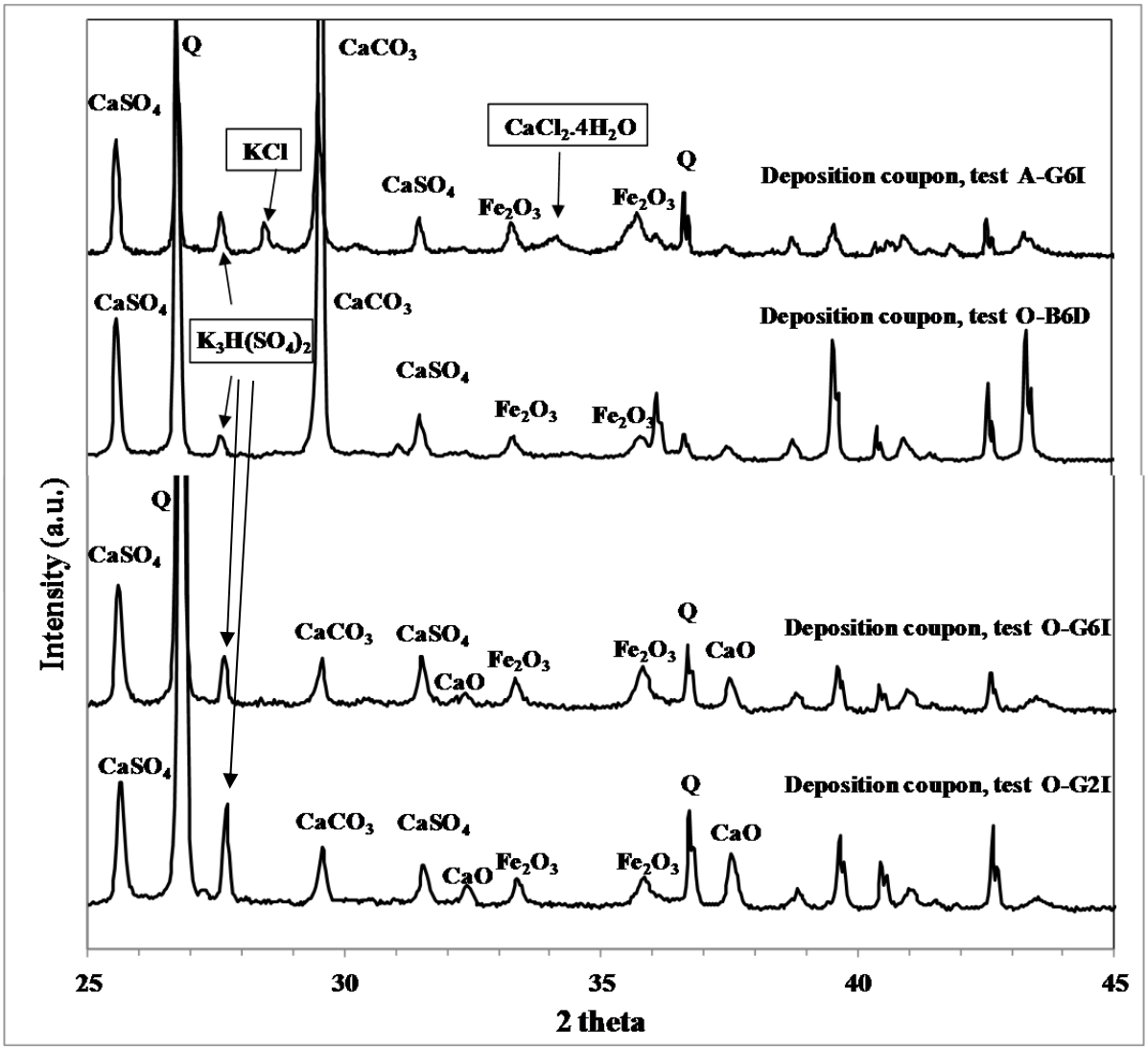

Figure 10. XRD composition of deposits formed during tests A-G6I, O-G6I, O-G2I and O-B6D.

Summing sections 3.2 and 3.3, it is concluded that oxy-firing barely affects the deposition rates in comparison to air-firing. Some increase of potassium sulphates in the deposits is observed for most of the oxy-firing tests, which can promote fouling after long-term operation. Nevertheless, and as a rule of thumb, no major operational problems are expected under oxy-combustion in comparison to the wide experience already available for air-fired operation of fluidized beds.

The composition of the deposits is fully consistent with the observed concentrations of SO_2 and HCl in the gas phase. The limestone type indirectly influences the composition of the deposits through the SO_2 concentration (largely determined by the limestone behaviour, as already discussed in section 3.1).

No influence of limestone has been observed on the composition of bed and fly ash. Lime chlorination – a positive side-effect – was found to a limited extent, but only for those tests with the higher deposition rates. Finally, agglomeration issues did not arise during the entire test campaign irrespective of the limestone used. Despite the addition of corn stover, and even for the higher temperature tests, operation of the fluidized-bed reactor is proven to be feasible for the blend of risky fuels selected.

3.4. Corrosion

Oxidation scales were only detected in experiments A-G6I and O-B6I. In the air case, removing the deposits by gentle brushing involved the collection of oxidation scales, as studied by SEM-EDX (Figure 11.a). The oxidation scale comprises a dual layer of Cr_2O_3-Fe_2O_3, which is expected from the high chromium content in AISI 304 stainless steel. The micrograph also shows the deposited material on the scale. Figure 11.b shows the condensed aerosols in the submicron range, the detailed composition of which by EDX is described in Figure 11.c. The aerosols are rich in Cl (16.1% atomic basis), K (13.5%), Ca (12.7%) and S (6.4%), with the rest composed of oxygen, which indicates the nucleation and condensation of a mixture of KCl, $CaCl_2$, and K-Ca sulphates. It has been stated that, in contrast to KCl, $CaCl_2$ is only slightly corrosive to SS304 under similar conditions [63].

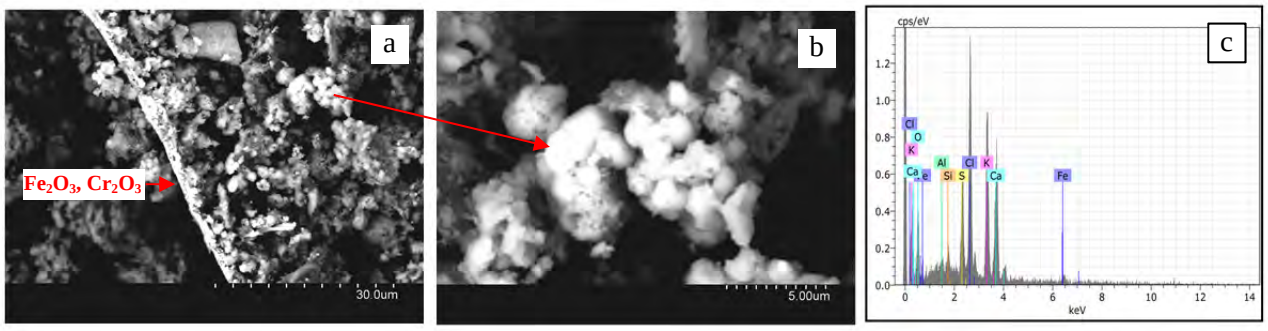

Figure 11. Deposit material from test A-6GI: (a) perpendicular view of the scale and deposit onto it; (b) details of the condensed aerosol cluster; (c) EDX composition of (b).

In the case of the O-6BI coupon, the fine deposit layer was washed off and the metallic surface was shown to be severely damaged by oxidation (Figure 12.a). SEM-EDX showed the spalled surface and, underneath, the formation of iron oxides that were rich in iron (Figure 12.b), which confirms the spallation of Fe_2O_3-Cr_2O_3 external scales and the formation of oxides, such as hematite, close to the metallic surface. These results demonstrate the incidence of accelerated corrosion due to the presence of KCl in deposits from the two tests with the highest degree of sulphur retention.

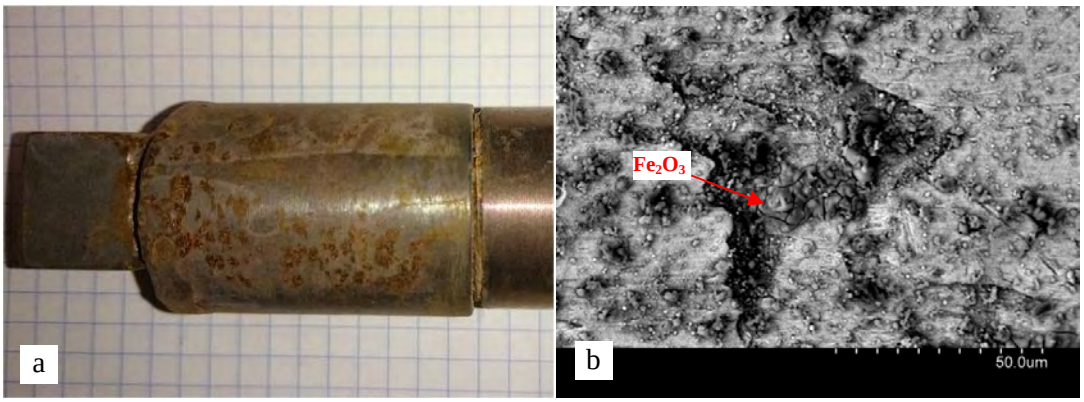

Figure 12. a) Washed deposition probe from test O-B6I; (b) and a detailed SEM micrograph.

In summary, oxy-firing is proven to alleviate corrosion issues compared to air operation. Only the test with the highest limestone fragmentation under calcining conditions yields a situation comparable to that observed for air. The results found in this work show the inter-relation between the type of limestone (determining the SO_2 concentration, and depending on the desulphurization mechanism) and mineral matter of coal and biomass (involving the alkali chlorides) under different, realistic operating

478 oxy-firing conditions. Again, non-calcining conditions are preferable, provided that a
479 large enough Ca:S ratio is used to achieve a high desulphurization efficiency.

480 ## 4. Conclusions

481 The influence of the type of limestone and desulphurization mechanism on emissions,
482 ash composition, deposition and corrosion were discussed after an experimental
483 campaign carried out under lab-scale fluidized bed oxy-firing conditions, feeding a blend
484 of lignite and corn stover.

485 SO_2 capture is better under calcining conditions than under non-calcining ones, but the
486 limestone type also has an outstanding relevance depending on the fragmentation
487 behaviour. Operation under calcining conditions requires higher bed temperatures
488 under oxy-firing, so there is a risk of agglomeration when supplying biomass in the
489 blend. However, no agglomeration was found for any of the tested conditions.

490 By contrast, NO_x emissions are increased under calcining conditions due to the catalytic
491 effect of free lime. This can be problematic for enriched O_2 atmospheres and when
492 supplying biomass with a nitrogen content higher than that of coal. Hence, a
493 compromise has to be adopted to jointly control the amounts of SO_2 and NO_x emitted.

494 Higher desulphurization efficiencies also promote the presence of chlorine in the
495 deposits, thus the risk of corrosion. This was detected for the air- and oxy-fired tests,
496 with efficiencies over 97%, but with more severe damage after the air-fired test.

497 Alkali sulfation was found for the tests with higher SO_2 contents, in agreement with the
498 HCl concentration in the gas phase, while alkali aluminosilication was shown to be
499 almost the same, irrespective of the atmosphere or operating conditions. Condensation
500 of potassium sulphates promotes deposition and increases fouling rates. Instead, the
501 risk of chlorine-induced corrosion is reduced.

502 The bottom ash is also free of chlorine due to its volatility. Finally, lime chlorination is
503 detected for the tests under calcining conditions, while limestone chlorination was not
504 found for the non-calcining tests.

505

506

Acknowledgements

The work described in this paper was partially funded by the R+D Spanish National Program from the Spanish Ministry of Economy and Competitiveness, under the Project ENE2012-39114. The project is also co-funded by the European Commission (European Regional Development Funds).

References

[1] Stanger R, Wall T, Spörl R, Paneru M, Grathwohl S, Weidmann M, et al. Oxyfuel combustion for CO_2 capture in power plants. Int J Greenh Gas Control 2015;40:55–125.

[2] Scheffknecht G, Makhadmeh LA, Schnell U, Maier J. Oxy-fuel coal combustion—a review of the current state-of-the-art. Int J Greenhouse Gas Con 2011;5S:16–35.

[3] Singh RI, Kumar R. Current status and experimental investigation of oxy-fired fluidized bed. Renew. Sustain. Energy Rev. 2016; 61: 398–420.

[4] Lupion M, Diego R, Loubeau L, Navarrete B. CIUDEN CCS Project: Status of the CO_2 capture technology development plant in power generation. Energy Procedia 2011;4:5639–46.

[5] Anheden M, Burchhardt U, Ecke H, Faber R, Jidinger O, Giering R, et al. Overview of operational experience and results from test activities in Vattenfall's 30 MW_{th} oxyfuel pilot plant in Schwarze Pumpe. Energy Procedia 2011;4:941–50.

[6] Uchida T, Goto T, Yamada T, Kiga T, Spero C. Oxyfuel Combustion as CO_2 Capture Technology Advancing for Practical Use - Callide Oxyfuel Project. Energy Procedia 2013;37:1471–9.

[7] Luo W, Wang Q, Liu Z, Zheng C. Dynamic simulation and exergy analysis for mode switching process in a 35 MW_{th} oxyfuel pilot plant. 5th Oxy-fuel Combust. Res. Netw. Meet., Wuhan (China): 2015.

[8] Bu CS, Gomez-Barea A, Chen XP, Leckner B, Liu DY, Pallares D, Lu P. Effect of CO_2 on oxy-fuel combustion of coal-char particles in a fluidized bed: Modeling and comparison with the conventional mode of combustion. Appl Energy 2016; 177:247-259.

[9] Yin CG, Yan JY. Oxy-fuel combustion of pulverized fuels: Combustion

fundamentals and modeling. Appl Energy 2016; 162: 742-762.

[10] Li SY, Xu MX, Jia LF, Tan L, Lu QG. Influence of operating parameters on N_2O emission in O_2/CO_2 combustion with high oxygen concentration in circulating fluidized bed. Appl Energy 2016; 173: 197-209

[11] Oboirien BO, Thulari V, North BC. Enrichment of trace elements in bottom ash from coal oxy-combustion: Effect of coal types. Appl Energy 2016; 177: 81-86

[12] de Diego LF, de las Obras-Loscertales M, Rufas A, Garcia-Labiano F, Gayan P, Abad A, Adanez J. Pollutant emissions in a bubbling fluidized bed combustor working in oxy-fuel operating conditions: Effect of flue gas recirculation. Appl Energy 2013;102: 860-867

[13] Vicente ED, Tarelho LAC, Teixeira ER, Duarte M, Nunes T, Colombi C, et al. Emissions from the combustion of eucalypt and pine chips in a fluidized bed reactor. J Environ Sci 2016;42:246–58.

[14] Khan AA, de Jong W, Jansens PJ, Spliethoff H. Biomass combustion in fluidized bed boilers: Potential problems and remedies. Fuel Process Technol 2009;90:21–50.

[15] Davidsson KO, Åmand L-E, Elled A-L, Leckner B. Effect of cofiring coal and biofuel with sewage sludge on alkali problems in a circulating fluidized bed boiler. Energy & Fuels 2007;21:3180–8.

[16] Pickard S, Daood SS, Nimmo W, Lord R, Pourkashanian M. Bio-CCS: co-firing of established greenfield and novel, brownfield biomass resources under air, oxygen-enriched air and oxy-fuel conditions. Energy Procedia 2013;37:6062–9.

[17] Schakel W, Meerman H, Talaei A, Ramírez A, Faaij A. Comparative life cycle assessment of biomass co-firing plants with carbon capture and storage. Appl Energy 2014;131:441–67.

[18] Gładysz P, Ziębik A. Environmental analysis of bio-CCS in an integrated oxy-fuel combustion power plant with CO_2 transport and storage. Biomass and Bioenergy 2016;85:109–18.

[19] Agbor E, Zhang X, Kumar A. A review of biomass co-firing in North America. Renewable and Sustainable Energy Reviews 2014; 40:930–943

[20] Sami M, Annamalai K, Wooldridge M. Co-firing of coal and biomass fuel blends. Progress in Energy and Combustion Science 2001; 27:171–214

570 [21] Valmari T, Lind TM, Kauppinen EI, Sfiris G, Nilsson K, Maenhaut W. Field study
571 on ash behavior during circulating fluidized-bed combustion of biomass. 2. Ash
572 deposition and alkali vapor condensation. Energy & Fuels 1999;13:390–5.
573 [22] Sandberg J, Karlsson C, Fdhila RB. A 7-year long measurement period
574 investigating the correlation of corrosion, deposit and fuel in a biomass fired
575 circulated fluidized bed boiler. Appl Energy 2011;88:99–110.
576 [23] Olivas-Ogaz MA, Paz MD, Liske J, Jonsson T. The effect of startup procedure of
577 probe exposures on deposit and corrosion formation in a waste fired CFB boiler.
578 22nd Fluid. Bed Convers., Turku (Finland): 2015.
579 [24] Niu SL, Han KH, Lu CM. Characteristic of coal combustion in oxygen/carbon
580 dioxide atmosphere and nitric oxide release during this process. Energy Convers
581 Manag 2011;52:532–7.
582 [25] Aho M, Ferrer E. Importance of coal ash composition in protecting the boiler
583 against chlorine deposition during combustion of chlorine-rich biomass. Fuel
584 2005;84:201–12.
585 [26] Akram M, Tan CK, Garwood DR, Fisher M, Gent DR, Kaye WG. Co-firing of
586 pressed sugar beet pulp with coal in a laboratory-scale fluidised bed combustor.
587 Appl Energy 2015;139:1–8.
588 [27] Barišić V, Peltola K, Coda Zabetta E. Role of pulverized coal ash against
589 agglomeration, fouling, and corrosion in circulating fluidized-bed boilers firing
590 challenging biomass. Energy & Fuels 2013;27:5706–13.
591 [28] Shao Y, Xu C, Zhu J, Preto F, Wang J, Tourigny G, et al. Ash and chlorine
592 deposition during co-combustion of lignite and a chlorine-rich Canadian peat in a
593 fluidized bed – Effects of blending ratio, moisture content and sulfur addition.
594 Fuel 2012;95:25–34.
595 [29] de Diego LF, de las Obras-Loscertales M, García-Labiano F, Rufas A, Abad A,
596 Gayán P, et al. Characterization of a limestone in a batch fluidized bed reactor for
597 sulfur retention under oxy-fuel operating conditions. Int J Greenh Gas Control
598 2011;5:1190–8.
599 [30] Liu H, Katagiri S, Kaneko U, Okazaki K. Sulfation behavior of limestone under
600 high CO_2 concentration in O_2/CO_2 coal combustion. Fuel 2000;79:945–53.
601 [31] de Diego LF, Rufas A, García-Labiano F, de las Obras-Loscertales M, Abad A,

602 Gayán P, et al. Optimum temperature for sulphur retention in fluidised beds
603 working under oxy-fuel combustion conditions. Fuel 2013;114:106–13.
604 [32] Díez LI, Lupiáñez C, Guedea I, Bolea I, Romeo LM. Anthracite oxy-combustion
605 characteristics in a 90 kW_{th} fluidized bed reactor. Fuel Process Technol
606 2015;139:196–203.
607 [33] Skeen SA, Kumfer BM, Axelbaum RL. Nitric Oxide Emissions during Coal and
608 Coal/Biomass Combustion under Air-Fired and Oxy-fuel Conditions. Energy &
609 Fuels 2010;24:4144–52.
610 [34] Riaza J, Gil MV, Álvarez L, Pevida C, Pis JJ, Rubiera F. Oxy-fuel combustion of
611 coal and biomass blends. Energy 2012;41:429–35.
612 [35] Moroń W, Rybak W. NO_x and SO_2 emissions of coals, biomass and their blends
613 under different oxy-fuel atmospheres. Atmos Environ 2015;116:65–71.
614 [36] Pickard SC, Daood SS, Pourkashanian M, Nimmo W. Co-firing coal with biomass
615 in oxygen- and carbon dioxide-enriched atmospheres for CCS applications. Fuel
616 2014;137:185–92.
617 [37] Jurado N, Darabkhani HG, Anthony EJ, Oakey JE. Oxy-combustion Studies Into
618 the Co –Firing of Coal and Biomass Blends: Effects on Heat Transfer, Gas and
619 Ash Compositions. Energy Procedia 2014;63:440–52.
620 [38] Ekvall T. Alkali sulphation in flames. 5th Meeting IEAGHG Int. Oxyfuel
621 Combustion Res. Netw., Wuhan (China): 2015.
622 [39] Ekvall T, Normann F, Andersson K, Johnsson F. Modeling the alkali sulfation
623 chemistry of biomass and coal co-firing in oxy-fuel atmospheres. Energy & Fuels
624 2014;28:3486–94.
625 [40] Tan Y, Jia L, Wu Y. Some combustion characteristics of biomass and coal cofiring
626 under oxy-fuel conditions in a pilot-scale circulating fluidized combustor. Energy
627 & Fuels 2013;27:7000–7.
628 [41] Duan L, Duan Y, Zhao C, Anthony EJ. NO emission during co-firing coal and
629 biomass in an oxy-fuel circulating fluidized bed combustor. Fuel 2015;150:8–13.
630 [42] Kosowska-Golachowska M, Wolski K, Kijo-Kleczkowska A, Musiał T, Środa K.
631 Experimental research on oxy-fuel combustion of biomass in a circulating
632 fluidized-bed. 7th Eur. Combust. Meet. (ECM 2015), Budapest (Hungary): 2015.
633 [43] Sengeløv LW, Hansen TB, Bartolomé C, Wu H, Pedersen KH, Frandsen FJ, et

634 al. Sulfation of condensed potassium chloride by SO_2. Energy & Fuels
635 2013;27:3283–9.
636 [44] Anthony EJ, Granatstein DJ. Sulfation phenomena in fluidized bed combustion
637 systems. Prog Energy Combust Sci 2001;27:215–36.
638 [45] de Diego LF, de las Obras-Loscertales M, Rufas A, García-Labiano F, Gayán P,
639 Abad A, et al. Pollutant emissions in a bubbling fluidized bed combustor working
640 in oxy-fuel operating conditions: Effect of flue gas recirculation. Appl Energy
641 2013;102:860–7.
642 [46] Wu Y, Wang C, Tan Y, Jia L, Anthony EJ. Characterization of ashes from a 100
643 kW_{th} pilot-scale circulating fluidized bed with oxy-fuel combustion. Appl Energy
644 2011;88:2940–8.
645 [47] Jia L, Tan Y, Anthony EJ. Emissions of SO_2 and NO_x during oxy−fuel CFB
646 combustion tests in a mini-circulating fluidized bed combustion reactor. Energy &
647 Fuels 2010;24:910–5.
648 [48] Valverde JM, Sánchez-Jiménez PE, Pérez-Maqueda LA. Limestone calcination
649 nearby equilibrium: Kinetics, CaO crystal structure, sintering and reactivity. J
650 Phys Chem C 2015;119:1623–41.
651 [49] Adánez J, De Diego LF, Gayán P, Armesto L, Cabanillas A. Modelling of sulfur
652 retention in circulating fluidized bed combustors. Fuel 1996;75:262–70.
653 [50] Zijlma GJ, Jensen AD, Johnsson JE, van den Bleek CM. NH_3 oxidation catalysed
654 by calcined limestone—a kinetic study. Fuel 2002;81:1871–81.
655 [51] Zijlma GJ, Jensen AD, Johnsson JE, van den Bleek CM. NH_3 oxidation catalyzed
656 by partially sulphated limestone—modelling and experimental work. Fuel
657 2004;83:237–51.
658 [52] Zijlma GJ, Jensen A, Johnsson JE, van den Bleek CM. The influence of H_2O and
659 CO_2 on the reactivity of limestone for the oxidation of NH_3. Fuel 2000;79:1449–54.
660 [53] Liu H, Gibbs BM. The influence of calcined limestone on NO_x and N_2O emissions
661 from char combustion in fluidized bed combustors. Fuel 2001;80:1211–5.
662 [54] Hansen PFB, Dam-Johansen K, Johnsson JE, Hulgaard T. Catalytic reduction on
663 NO and N_2O on limestone during sulfur capture under fluidized bed combustion
664 conditions. Chem Eng Sci 1992;47:2419–24.
665 [55] Lupiáñez C, Díez LI, Romeo LM. NO emissions from anthracite oxy-firing in a

666 fluidized-bed combustor: Effect of the temperature, limestone, and O_2. Energy &
667 Fuels 2013;27:7619–27.
668 [56] Niu Y, Tan H, Hui S. Ash-related issues during biomass combustion: Alkali-
669 induced slagging, silicate melt-induced slagging (ash fusion), agglomeration,
670 corrosion, ash utilization, and related countermeasures. Prog Energy Combust Sci
671 2016;52:1–61.
672 [57] Lupiáñez C, Mayoral MC, Guedea I, Espatolero S, Díez LI, Laguarta S, Andrés
673 JM. Effect of co-firing on emissions and deposition during fluidized bed oxy-
674 combustion. Fuel 2016;184:261–68.
675 [58] García-Labiano F, Rufas A, de Diego LF, de las Obras-Loscertales M, Gayán P,
676 Abad A, et al. Calcium-based sorbents behaviour during sulphation at oxy-fuel
677 fluidised bed combustion conditions. Fuel 2011;90:3100–8.
678 [59] Laursen K, Duo W, Grace J., Lim J. Sulfation and reactivation characteristics of
679 nine limestones. Fuel 2000;79:153–63.
680 [60] Shemwell B, Levendis YA, Simons GA. Laboratory study on the high-temperature
681 capture of HCl gas by dry-injection of calcium-based sorbents. Chemosphere
682 2001;42:785–96.
683 [61] Partanen J, Backman P, Backman R, Hupa M. Absorption of HCl by limestone in
684 hot flue gases. Part III: simultaneous absorption with SO. Fuel 2005;84:1685–94.
685 [62] Wang W, Li Y, Xie X, Sun R. Effect of the presence of HCl on cyclic CO_2 capture of
686 calcium-based sorbent in calcium looping process. Appl Energy 2014;125:246–53.
687 [63] Karlsson S, Pettersson J, Johansson L-G, Svensson J-E. Alkali induced high
688 temperature corrosion of stainless steel: The influence of NaCl, KCl and $CaCl_2$.
689 Oxid Met 2012;78:83–102.

690
691
692